ROTATIONAL 3D PRINTING OF SENSOR DEVICES USING REACTIVE INK CHEMISTRIES

C. Hauser [a], D.M. Lewis [b], K.F. Morris [b], P.J Broadbent [b] , X. Zhao [b],
A.T. Clare [a] and M. Dunschen [c].
[a] MSERC, Department of Engineering, University of Liverpool, UK
[b] Department of Colour and Polymer Chemistry, University of Leeds, UK
[c] FreeSteel, Liverpool, UK

Abstract

This paper charts progress in three key areas of a project supported by both UK government and UK industry to manufacture novel sensor devices using rotary 3D printing technology and innovative ink chemistries; (1) the development of an STL file slicing algorithm that returns constant Z height 2D contour data at a resolution that matches the given print head setup, allowing digital images to be generated of the correct size without the need for scaling; (2) the development of image transformation algorithms which allow images to be printed at higher resolutions using tilted print heads and; (3) the formulation of multi part reaction inks which combine and react on the substrate to form solid material layers with a finite thickness. A Direct Light Projection (DLP) technique demonstrated the robustness of the slice data by constructing fine detailed three dimensional test pieces which were comparable to identical parts built in an identical way from slice data obtained using commercial software. Material systems currently under investigation include plaster, stiff polyamides and epoxy polymers and conductive metallic's. Early experimental results show conductivities of silver approaching $1.42x10^5$ Siemens/m.

Introduction

Three Dimensional Printing (3DP) was developed at the Massachusetts Institute of Technology in the late 1980's [1]. It is a layered manufacturing process that builds parts by the repetitive deposition of thin powder layers, regions of which are selectively solidified by inkjet printing a binder from a scanning print head. The application of the binder also bonds consecutive layers together. In a final processing step, parts are often infiltrated with resin or wax to increase strength and durability [2]. In this work a different approach is being adopted. It is driven by the need for a 3D micro-fabrication printing process that firstly, allows multiple material systems to be printed in the same layer without the need to deposit powder, secondly, increases part accuracy and thirdly, utilises industrial print heads and a rotary substrate to maximise build speed [3]. The print heads are wide format OmniDot 760 industrial print heads, capable of printing a 53.8mm print swathe in a single pass from 764 nozzles (360dpi), and are supplied by XaarJet Ltd, UK. The applications are novel gas and induction sensors which require both conductive coatings and insulating structures capable of performing at elevated temperatures. Their geometries are complex and include geometric features with sizes that range from 200 microns to 2mm. At the time of writing this paper there were a number of patent issues surrounding the sensors and their proposed methods of manufacture. Therefore, detailed descriptions of the sensors are restricted at this time.

The novel manufacturing route proposed would allow increased sensitivity and further miniaturisation in both sensor technologies. A unique interdisciplinary team with skills in manufacturing, electronics, software and systems integration and ink formulation has been

established to ensure this challenging programme is successful. This paper details some early developments in this work. Firstly, the development of an STL format slicing algorithm is reported that decomposes the 3D model into two dimensional layers by calculating contour data, at a predefined resolution, by intersecting the model with parallel vectors at constant Z height in the xy plane. The majority of previous work has concentrated on adaptive slicing techniques that regulate slice resolution only in the Z direction to optimise geometry and reduce the effect of stair step [4]. Vogt et al. [5] took their slicing algorithm a stage further and superimposed a high, but limited, resolution pattern generator, or mesh structure, on the 2D contour data to calculate xy contour points at intersecting nodes. Bitmap images were then created for a Microstereolithography process at the same resolution of the pattern generator. For the present, slicing algorithm, the resolution of the slice in the xy plane is adapted to suit printing requirements, and the resolution is unlimited (although ultimately governed by the resolution of the STL file). This facilitates the generation of digital images at the required resolution without the need for scaling. Hence, the software can be used to test for part design integrity by resolving the minimum feature size that can be printed for a given hardware setup. Complex, and small scale, 3D geometries used for performance tests were sliced and built using an EnvisionTec Perfactory computer aided modelling device (see *Equipment and Experimental Methods* Section) [6].

Secondly, the development of a transformation algorithm that geometrically transforms digital images in preparation for printing onto a rotary substrate using off axis or tilted print heads is reported. The work has both an application and a fundamental purpose. The application purpose is to investigate the feasibility of increasing print head resolution by tilting the print head away from the printing direction. The theory driving this work is the ability to print finer geometric features and extends research conducted by XaarJet to investigate image clarity when printing digital media using tilted OmniDot 760 print heads; their results were inconclusive. In their work image transformation algorithms were not implemented. The fundamental purpose is to gain better understanding of the effects of print head setup, print density and non-conventional printing methods on printed image accuracy and clarity. This work may also be of interest in areas of conventional linear printing. It is important to note here that this work establishes methods to change position of droplets on the substrate and does not consider, at this stage, changes in printing behaviour that might result from varying printing conditions.

Thirdly, this paper discusses work in progress on the development of novel ink chemistries that are capable of inkjet printing Plaster of Paris, various polymers and metallic materials. All ink development work was conducted using a HP DeskJet printers.

STL Slicing Algorithm

The slicing algorithm reported in this work has evolved from a machining algorithm based on CAM-style slicing with a defined tool shape. This code (written in C++ and Python) has been developed by Freesteel (www.freesteel.co.uk), developers of algorithms used widely in the CAM industry. Conventionally CAM requires the specification of a tool geometry; a cylindrical shape with a torus, spherical or flat tool tip at the bottom. The Freesteel (FS) slicer divides this tool shape into several parts: a tip (sphere, torus, or flat disk), an optional shaft (cylindrical or conical) and optionally any number of cylindrical or conical holder shapes. The shaft diameter is not restricted to the tip diameter; a shaft smaller than the tip, for example, can

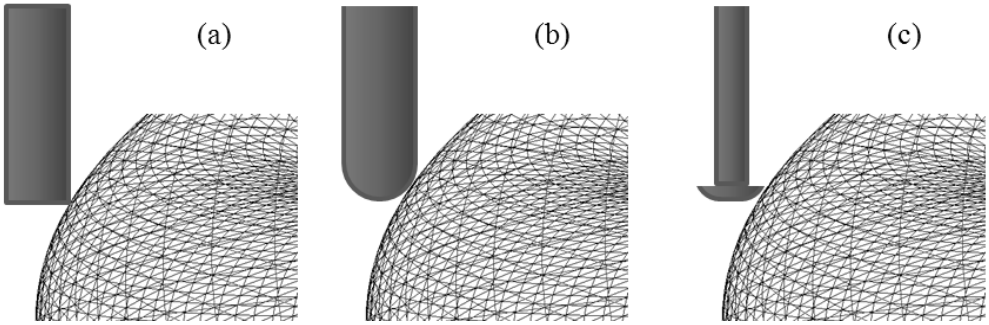

Figure 1: FS slicer tool geometry: (a) flat tool tip, (b) spherical tool tip and (c) torus tool tip and small cylindrical shaft (lollipop).

be used to model lollipop cutters. Contours, or tool paths, are calculated for the tip centre so that when the tool shape is positioned anywhere along the calculated contour the STL will touch this tool tip (see Figure 1).

In order for contours resulting from this algorithm to coincide with the STL geometry at a given Z height they have to be offset inwards. For a flat bottom tool tip the offset amount equals the tool radius, but for spherical or toroidal shapes the offset depends on the distance between contact point and STL. If a shaft shape was specified the algorithm would continually 'look up' for triangles above the slice height that could interfere with the tool shaft, hence the algorithm would not model any undercuts of the STL (This is a desired feature of 3 axis tool paths).

By restricting the tool geometry to the tip shape FS slicer can model undercuts, but the resulting contours have to be processed through 2 steps: (1) Unwanted contours "inside" the volume modelled by the STL have to be filtered out (the algorithm would pass the tool along both sides of the contour because any triangles above the tip will not interfere with this tip) and (2) an inward offset has to be applied because contours are referenced to the centre of the tool (see Figure 2). Also, if there are many sloping angles the tool contact point would move around the tool geometry and offset parameters would need recalculating. The use of this area based algorithm is also restricted to the use of tools with a finite dimension. This method is appropriate for machining operations and may also be useful for SFF technologies that use a tool with a finite area to process each layer i.e. laser processing as one example. However, the slice images required for this project need to resemble, as accurate as possible, the underlying STL geometry; a dimensionless tool would give this accuracy. There are also a number of other disadvantages this approach brings i.e. filtering of unwanted contours and offsetting, all of which increase the time to slice.

For reasons giving above, the FS slicer was developed further to offer the calculation of intersections of a 1 dimensional vector or 'fibre' through the STL triangulation, and these intersections can be calculated for a dimensionless or point tool shape. By calculating a series of parallel fibres at constant Z height, for example, fibres incremented by a distance equal to that of the frequency of nozzles across the print head, the model can reciprocate exactly a given printer setup (see Figure 3). As each fibre passes through the STL model the algorithm counts intersections and assumes the first represents a move from outside to inside and a second from inside to outside, thereafter the methodology repeats.

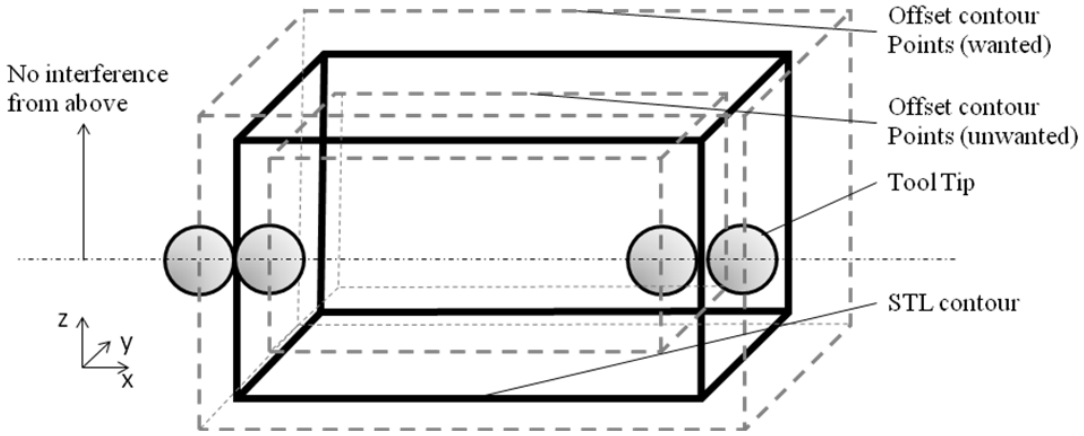

Figure 2: FS Slicer with spherical tool tip processing four contours, two unwanted and two requiring to be offset inwards.

In Figure 3a, a generic STL model is shown with intersecting fibres positioned at 3mm intervals. Point data collected from this model was used to generate a digital 2D image sized to correspond to the native resolution of the OmniDot 760 print head i.e. 14.2 pixels/mm (764 nozzles/ 53.8mm). The image, given in Figure 3b, is clearly incomplete due to the inadequate fibre resolution, giving a partial image with data visible only in every 42nd row of pixels. For accurate and compete image reconstruction at this resolution, the fibre interval would need to reduce to 0.07mm (1/14.2), as used to generate the digital image in Figure 3c. Capturing slice data is this way allows finite detail to be resolved, but only within limits of the print head setup; maximising efficiency of the time to slice. It also increases accuracy by removing the need to interpolate between data points or scale an image when high resolution images are required. The FS fibres can also orientate at any angle to model the print output in different directions which may facilitate optimal part orientation in preparation for a build.

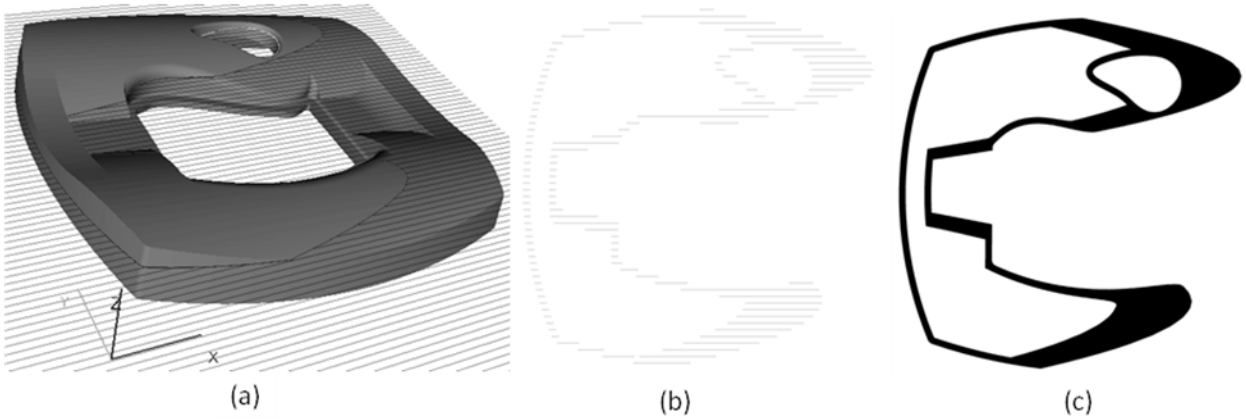

Figure 3: (a) STL model showing FS Slicer scan lines at 3mm spacing and constant Z height, (b) bitmap image generated from sliced data obtained from (a) and (c) bitmap image generated from sliced data obtained from scan lines with 0.07mm spacing.

Image Transformations

To successfully print an image using SGM, images must first undergo a series of geometric transformations The method has been published previously [3], for radially aligned print heads. It is the changes need to apply the algorithms for off axis or tilted print heads that are discussed in the following. The previous work developed two image transformation algorithms, firstly the polar transformation to correct for the annular distortion of images when printed onto a rotary substrate and secondly, a linear transformation in which columns of pixels were displaced to correct for a parallax shift caused by the dual nozzle row design of the chosen print head (see later). In this work the linear transformation is adapted to take into account positions of nozzles, relative to the radial centre line, for a given angle of tilt. Python programming language was used in the development of the transformation algorithms [7].

The coordinate system used in the transformation calculations starts at, $x = 0, y = 0$, in the upper left corner of an image and the coordinates refer to positions between pixels. The position of pixels, P_t, in the transformed image are described in a similar manner but are distinguished by the Cartesian coordinates, *u,v*. The position of pixels in the printed transformed image are again described in *x,y*. In the OmniDot 760 print head there are two rows of nozzles. Each row contains 382 active nozzles that are positioned in an alternating manner so that a nozzle in one row is either to the left or the right of a nozzle in the other row. This arrangement, together with OEM software which offsets the start of firing of one row of nozzles, gives an effective print swathe containing 764 nozzles (ps_{nz}) over a distance of 53.8mm (ps_{mm}). This gives a print resolution of 360dpi or 14.2pixels/mm across the print head, and is orientated radially, dpi_x, in the SGM apparatus. The print density perpendicular to the print head, dpi_y, is the circumferential print density and is governed by the clocking frequency driving the print head. Typically, this can range between 200 dpi and 2000 dpi, and is dependant on the hardware setup. For the purposes of this work, $dpi_y = dpi_x = 360$, although images can be transformed for an unlimited range of aspect ratios. Finally, all measurements in this work are in pixels unless otherwise stated.

To start, an 8 bit greyscale or monochrome image of size, *sx, sy*, is numerically positioned so that its central horizontal axis aligns with the centreline, *CL*, about which the print head is tilted (see Figure 4). The first column of pixels in the image are positioned at a radial distance of, $cx_T + px_T$. Where, cx_T, is the distance from the centre of rotation to the first nozzle in the lead nozzle row, *nzr1*, of the tilted print head and is given by:

$$cx_T = cx + \frac{\left(d_{nzr} \sin \theta_{PH}\right)}{2} \tag{1}$$

and, px_T, is the position of the image within the projected print swathe, ps_P. The size of the projected print swathe can be calculated using:

$$ps_p = ps.\cos \theta_{PH} - d_{nzr} \sin \theta_{PH} \tag{2}$$

Where, $d_{nzr} \sin \theta_{PH}$, is the length of the nozzle row containing redundant nozzles i.e. nozzles that do not coincide with nozzles in the opposing row. Hence, in this region the print

density would be half the projected print density, dpi_{xp}. dpi_{xp}, of the tilted print head can be calculated using:

$$\mathrm{dpi}_{xp} = 25.4 \times \frac{ps_{nz}}{ps_{mm}} \left(\frac{1}{\cos \theta_{PH}} \right) \tag{3}$$

The new image size, *su, sv,* is then calculated according to, dpi_{xp}, and, dpi_y, and the polar transformation algorithm, for a radius of, $cx_T + px_T$, moves each pixel from the original image into the new image by the method discussed in [3]. A graph plotting both, dpi_{xp}, and, ps_p, with changes in tilt angle is given in Figure 5. From the figure it is clear that the projected print swathe significantly diminished with large increases in projected print density. Furthermore, the maximum print angle occurs at, $\cos \theta_{PH} = d_{nzr} / ps$ = 85.5 degrees.

The next step is a linear transformation of the polar transformed image. In previous work [3] columns of pixels are remapped (or moved) in an alternating $\pm v$ direction to align the centreline of the image, *sy/2,* with the centre between nozzle rows i.e. CL (see Figure 4b). In this work, the linear transformation algorithm functions in a similar way, but the displacement of pixels is greater and variable across the projected print swathe because the centre between nozzle rows does not coincide with, CL.

The amplitude and direction of displacement for each column of pixels is a function of the radial position of the nozzle, the row in which the nozzle is located and the tilt angle of the print head. For, *nzr1*, the amplitude and direction changes linearly across the projected print swathe from, $coff_{01}$, to, $coff_{11}$, and from , $coff_{02}$, to, $coff_{12}$, in, *nzr2*, where (in this example sx = ps_p):

$$coff_{01} = -\frac{nzr_{off}}{2} \cdot \cos \theta_{PH} \ , \qquad coff_{11} = \left(sx \sin \theta_{PH} \right) + coff_{01} + \left(sx \tan \delta_{par} \right) \tag{4}$$

and

$$coff_{02} = \frac{nzr_{off}}{2} \cdot \cos \theta_{PH} \ , \qquad coff_{12} = \left(sx \sin \theta_{PH} \right) + coff_{02} - \left(sx \tan \delta_{par} \right) \tag{5}$$

Where, δ_{par}, is the angle of the parallax shift and is calculated using:

$$\delta_{par} = \tan^{-1} \left(\frac{d_{nzr}}{2(cx_T + px_T + sx)} \right) \tag{6}$$

An example digital image transformed using the techniques described in this work can be seen in Figure 6. Monochrome bitmap images of squares, rectangles and circles were transformed by methods discussed above and printed using a bench top rotary printing system to verify the dimensional accuracy of the printed images. The results were encouraging but further work using the more accurate SGM apparatus would be necessary. The effects on image clarity was not investigated in this work.

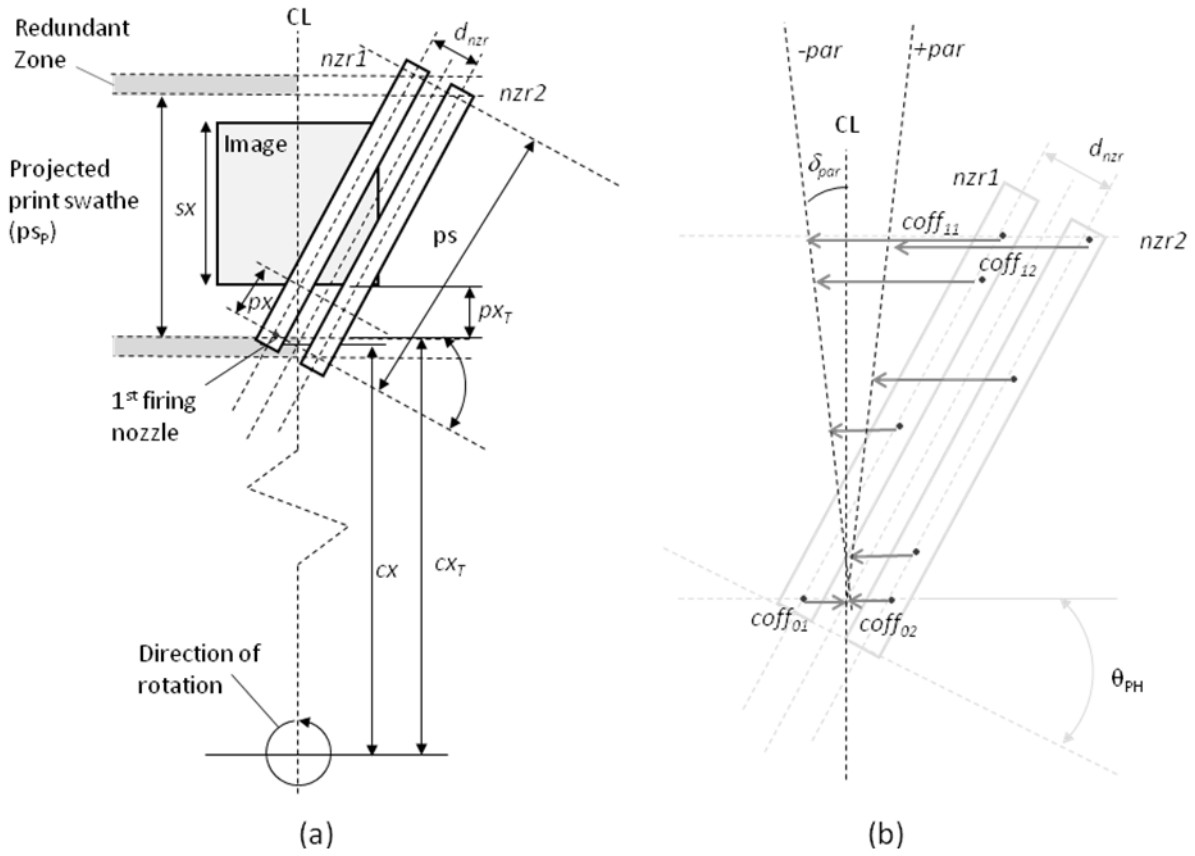

Figure 4: (a) Showing print head orientation and sign convention used in transformation calculations and (b) minimum and maximum nozzle offset values, $coff_{01}$, $coff_{11}$, $coff_{02}$ and $coff_{12}$.

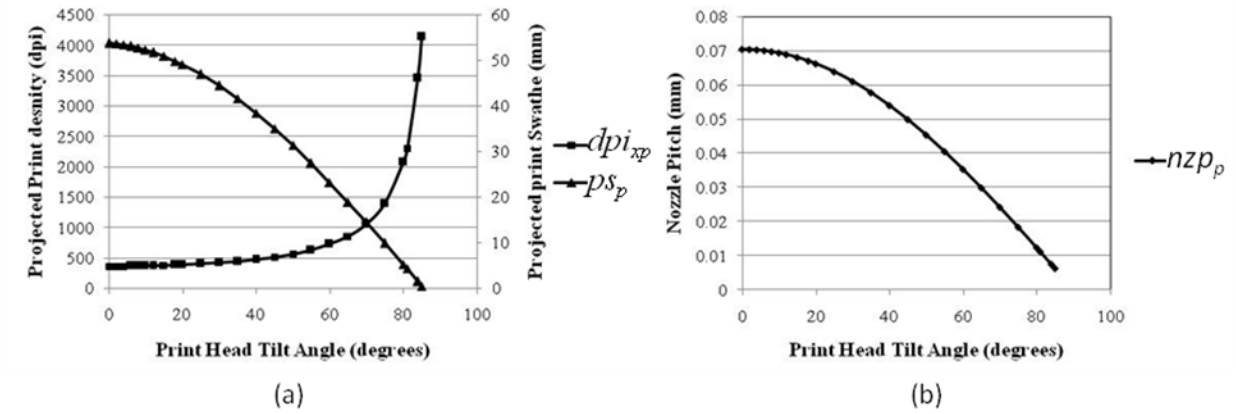

Figure 5: (a) Graph plotting print head tilt angle with projected print density, dpi_{xp}, and projected print swath, ps_p, and (b) graph plotting print head tilt angle with nozzle pitch.

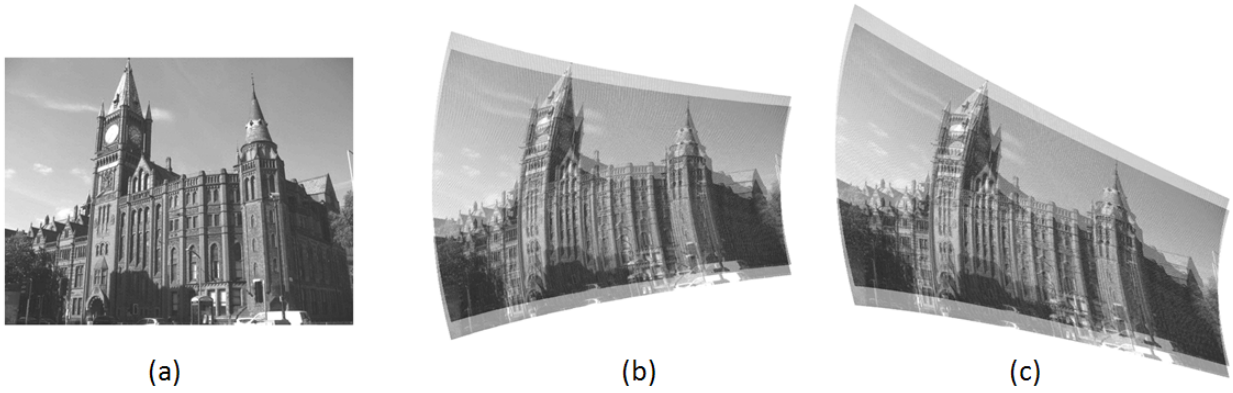

Figure 6: Polar-Linear image transformations (a) original image (b) transformed for aligned print head and (c) transformed for print head tilted at 20°.

Ink Development

Plaster Inks: Inovink [GB 0803234.4] has patented the use of Plaster of Paris pre-cursor chemistries to precipitate strong plasters ($CaSO_4$. 0.5 H_2O) from aqueous solutions; thus one ink-jet cartridge contains calcium chloride and the other ammonium sulphate; it is also necessary to adjust cartridge solutions to pH6-7. Typically, ammonium sulphate solutions are printed first and then the plaster is obtained by printing the calcium chloride solution. Thus far the most impressive results have been obtained using the HP office ink-jet printer but trials are in hand to engineer the solutions to fit commercial ink-jet heads such as those available for this project. In particular the ammonium sulphate solution needs reformulation to prevent crystallization on the print head causing nozzle blockages. Typical results are shown in Figure 7.

Polymer Inks: Research in this project has proven that it is very difficult to jet water-soluble polymers so it is a necessary part of further research to develop water-soluble pre-polymers which will either self cure to give high molecular weight rigid polymers or which will rapidly condense with diamines or dithiols to form solid high polymers. Some success has been achieved using a water-soluble poly-epoxide which is readily jettable and which cures to give a strong rigid high polymer. It would be advantageous if the use of a two component system could be avoided. Issues such as ink stability need to be resolved. A novel approach to two pack polymer-forming systems has been developed using acyl-thiol derivatives of acid chlorides which bear water solubilising functionality on the thiol residue. Such compounds react with poly-amines at room temperature to give polyamides. Polymers with high thermal stability are also being investigated.

Conductive Inks: Silver has been formed by ink-jet printing silver nitrate which is then reduced by over printing with ascorbate onto paper substrates (tests also be carried out in plaster substrates). The printed layer then needs to be flash heated at 150 degrees for approximately 1 minute. Conductivities of printed samples (on paper) were found to be in the region of $1.4x10^5$S/m (solid silver = $6.1x10^7$S/m). Once again silver test prints have been carried out using a HP office ink-jet printer.

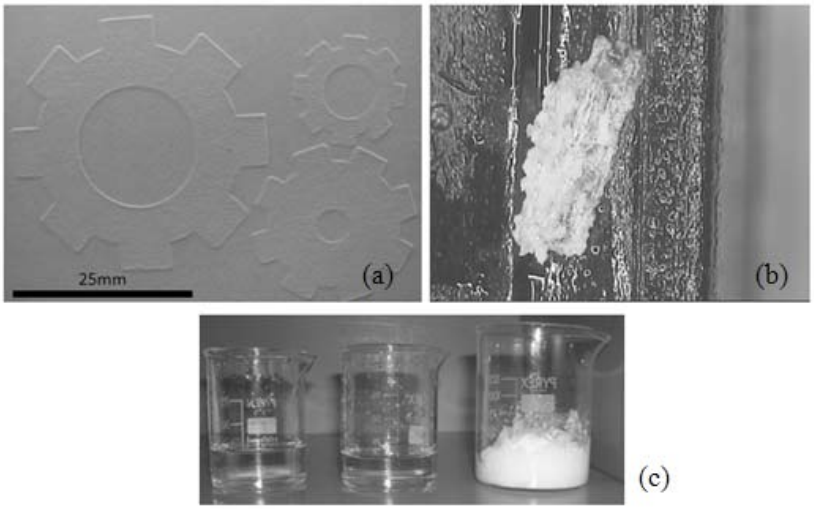

Figure 7: (a) Gear shapes printed by 3 passes with ammonium sulphate and last pass with calcium chloride, (b) crystallization of ammonium sulphate solution on Omnidot 760 print head and (c) beaker test showing precipitates of plaster when tipping calcium chloride solution into ammonium sulphate solution.

Equipment and Experimental Methods

The FS slicing algorithm has been performance tested experimentally by creating slice data from a three dimensional test component and fabricated using an EnvisionTec Perfactory SXGA (ETec) computer aided modelling device [6]. The component is 10mm square and 1.6mm high and contains a level of detail that makes it a good candidate as a demonstrator for sensor development trials (see Figure 9a). Comparisons are also made with similar test pieces built using ETec but orientated using the commercial software package Magics ™ [8] and then sliced and prepared using proprietary software (Perfactory RP 2) shipped with the ETec system. The ETec machine uses Digital Light Projection (DLP) technology to project UV light onto a photo-sensitive curable resin. In DLP projectors, the image is created by microscopically small mirrors laid out in a matrix on a semiconductor chip, known as a Digital Micromirror Device (DMD). Each mirror represents one pixel in the projected image and can be repositioned rapidly to reflect light either through a lens or onto a light dump. The ETec system can project an image with a resolution of 1400x1050 pixels, focused by two projection lenses onto a platform of size 27.77 x 20.83mm. Hence, the resolution of this system is likely to far exceed the resolution obtainable using the OmniDot 760 print heads. The FS slicer was adapted to slice and generate images at the required higher resolution (fibre resolution of 0.0198mm). Each image was then inverted to act as a mask i.e. areas of exposure were represented by white pixels and masked areas were represented by black pixels.

To engineer a fair comparison test it was important to be aware of several image processing techniques adopted by the ETec software to improve build accuracy. Firstly, ERM (Enhanced Resolution Mode) is often used to improve part integrity by processing each sliced layer twice, where each repeated layer is digitally offset from the first by shifting the image by one pixel in both x and y directions; an analogy would be building a brick wall where voxels in adjacent layers are staggered. Secondly, an edge smoothing algorithm is applied, for both ERM and non ERM masks, to improve part surface quality. Considering the second first, a standardised edge smoothing algorithm, available in Python Imaging Library [8], was

implemented in the FS slicer software to attempt to match images processed using the proprietary software, but output was slightly different (see Figure 8). The shape of the convolution kernel used in the smoothing algorithm was [(1,1,1),(1,5,1),(1,1,1)]. The FS slicer software was also adapted to offset alternate images by one pixel in both x and y directions. However, when cycling through the images at high speed the offset was visually more significant in the FS sliced images; probably caused by the differences in edge smoothing which also acted to conceal the offset. For this reason, FS image offsetting was not implemented in this work.

Four test builds were prepared; (P1) Perfactory with ERM on, (P2) Perfactory with ERM off, (FS1) FS Slicer with edge smoothing on and (FS2) FS slicer with edge smoothing off. The images or masks were saved in PNG graphics format necessary for projection via DLP. The file naming followed the propriety software method and masks obtained using the FS slicer were directly replaced with ETec masks in the generated job file (.JOB). A .TXT file which summarised processing parameters and a .CFG file which contained build parameters, also present within the .JOB file, were not edited.

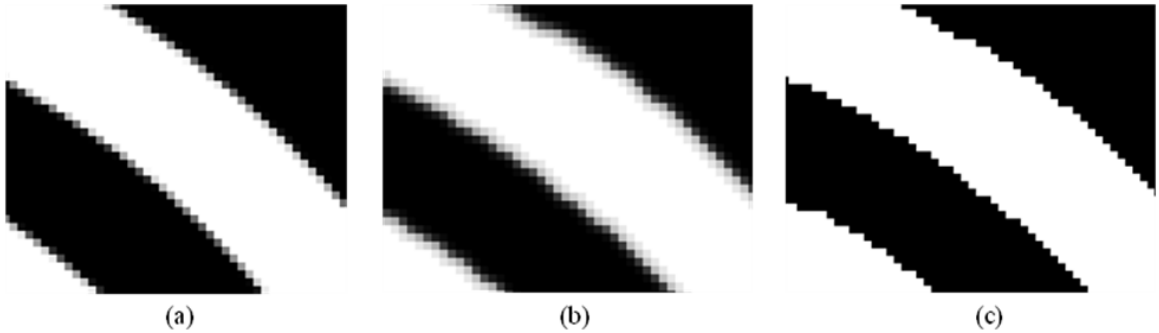

Figure 8: Bitmap slice data showing (a) ETec edge smoothing- PS1, (b) FS Slicer with edge smoothing on - FS1 and (c) FS Slicer with edge smoothing off –FS2. Magnification X600.

Experimental Results and Discussion

An Envisiontec Perfactory (ETec) standard system [6] was used to construct four identical test components PS1, PS2, FS1, and FS2. The experimental conditions are outlined in the *Equipment and Experimental Methods Section* of this paper. On visual inspection of all four parts, PS1 and FS1 were similar with good geometric reproducibility, edge definition and fine detail resolution. Conversely, PS2 and FS2 had poor edge definition and were generally considered to be inferior to PS1/FS1. The SEM images given in Figure 9d-g confirm the visual observations. However, smaller features in FS1 i.e. narrow walls and channels (10 - 50 microns in size), had failed to build correctly or had closed or were missing. An example can be seen in the failed wall section of the concentric circles feature on the left of Figure 9c. These observations are likely to be caused by the FS slicer edge smoothing algorithm. In Figure 8, it is clearly evident that the band of pixels with varying levels of grey running along the image boundary had a much wider profile in FS1 than in PS1. In particular, Figure 10, shows the section of mask which resulted in the failed wall of Figure 9c. In Figure 10 there is clearly a narrowing of higher intensity regions (white pixels) in the wall section of FS1. The combination of a small feature size and a reduction in exposure level across the feature is likely to promote pealing, where layers peel away from underlying layers.

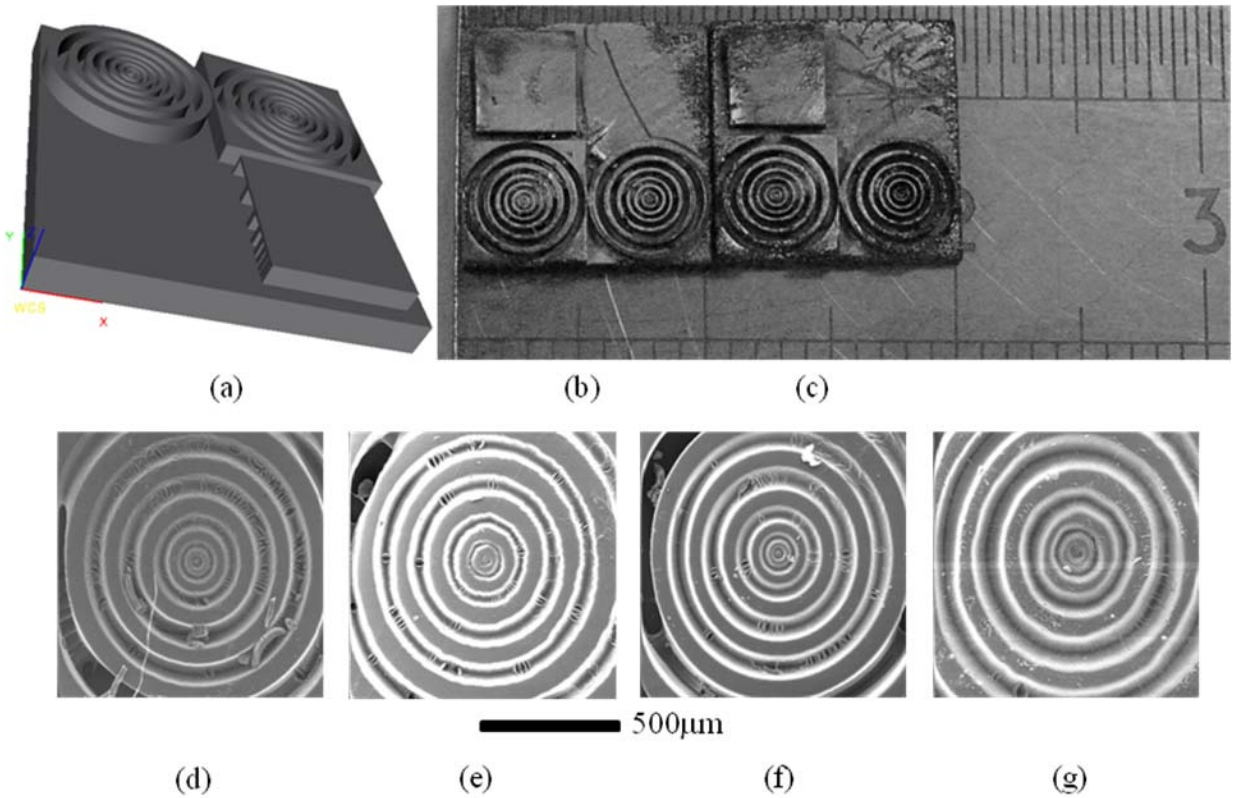

Figure 9: (a) STL model used for performance tests, (b) Gold coated component - PS1, (c) Gold coated component - FS1, (d) SEM image - PS2, (d) SEM image - FS2, (f) SEM image – PS1 and (g) SEM image – FS1.

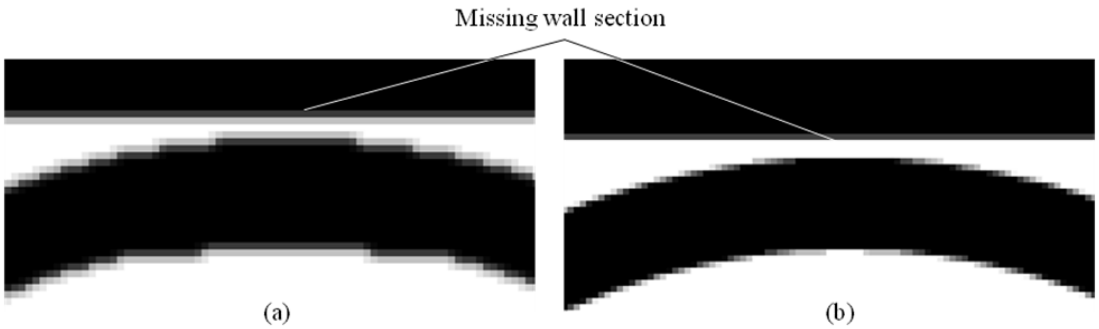

Figure 10: Layer masks showing edge of concentric circles feature in (a) FS1 and (b) PS1.

Conclusions

This paper has briefly reviewed several key areas of research within a project aimed at the development of a multiple material 3D micro-fabrication printing process. Firstly, an STL slicing algorithm has been written which tailors the resolution of the calculated contour data to match the resolution of the hardware i.e. a print head or projector. Slice data obtained from the FS slicer and from commercial software was used to construct comparable geometries. However, small features i.e. thin walls and channels, typically less than 50 microns, were missing in some regions of the FS sliced test pieces. The edge smoothing algorithm, which heavily blurred the transition across edge boundaries and altered UV light exposure levels, has been consider responsible for the missing features and not due to the way in which slice contour

data is collected and converted into a bitmap image using the FS slicing algorithm. Additional work is required to investigate the shape of the convolution kernel used in the ETec propriety software in the hope that the procedure can be duplicated or improved.

The polar transformation algorithms for tilted print heads has proven successful for accurate geometric reproduction of images of basic shapes (squares, triangles etc) when printed onto a rotating substrate. The clarity of image reproduction for more complex images and the droplet behaviour at the higher print densities, particularly at the point of impact with the travelling substrate still needs to be investigated. Furthermore, the transformation algorithms, which work on a pixel by pixel basis, tend to be rather slow and are dependant on image size and not on STL complexity (1200x1200 pixel images take approximately 8 seconds to process). A new combined FS slicing and transformation algorithm is under development and early indicators suggest speed increases of ~80%.

Ink developments are nearing to a working solution for the plaster forming inks in the Xaar print heads. Polymer systems have proved difficult from all aqueous solutions and so solvent based systems are now being investigated with the possible use of remedial steps i.e. heat treatment and UV curing. Conductivities of metal inks are currently to low for sensor applications. Improvements may be sought by printing onto specially prepared substrates. Conductivities may also improve when moving to Xaar print heads where higher print densities and greater accuracy during overprinting would become possible.

Acknowledgements

This work has been supported by UK Government and a number of UK industrial partners: Xaarjet Ltd, MCP Tooling Technologies Ltd, Zettlex Ltd and Inovink Ltd. One of us (Hauser) would also like to thank Martin Dunschen and Julian Todd from FreeSteel, UK (www.freesteel.co.uk), for developing the slicing algorithm and their support and advice with general programming issues.

References

[1] Sachs, E., Cornie, J., Brancazio, D., Bredt, J., Curodeau, A., Fan, T., Lauder, A., Lee, J. and Michaels, S. (1993). Three dimensional printing: the physics and implications of additive manufacturing. CIRP Annals, Vol.42, 1, pp. 257-260.

[2] Cooper, K.G., Williams, G., Salvail, P. (2002). Evaluating RP Methods: NASA's Side-by-Side Comparison. Proceedings Modern Casting, Feb. 2002, pp 28-30.

[3] Hauser, C., Lewis, D .M., Dunschen, M., Egan, M. and Sutcliffe, C. (2007). Image Transformations And Printing Of Plaster Layers in Spiral Growth Manufacturing. Proceedings of SFF, Austin, Texas.

[4] Choi, S.H. and Kwok, K.T. (2002). A tolerant slicing algorithm for layered manufacturing. Rapid Prototyping Journal, Volume 8, number 3. Pp. 161 – 179.

[5] Vogt, C., Bertsch, A., Renaud, P. and Bernhard, P. (2002). Methods and Algorithms for the Slicing Process in Microstereolithography. Rapid Prototyping Journal, Volume 8, number 3. Pp. 190 – 199.

[6] Website: http://www.envisiontec.de (accessed May 2008)

[7] Lutz, M. (2001). Programming Python – 2nd Edition. O'Reilly Media. ISBN 978-0596000851

[8] Website: http://www.materialise.com (accessed June 2008)

[9] Website: http://www.pythonware.com/products/pil/ (accessed July 2008).